Table of Contents

Study of Flexure-based Tiltmeter

2340413P

Abstract

This study involved finding the magnitude of dominant noise sources present in a beam rotation sensor, such as seismic and thermal noise present at low frequencies below 100 Hz and improving the signal to noise ratio. The noise was improved by changing parameters of the beam balance, such as the centre of mass, flexure stiffness, and quality factor. The beam rotation sensor was more efficient in distinguishing the coupling between platform rotation and acceleration than a horizontal seismometer or tiltmeter. However, below the resonant frequency of the system, the measured output was less than the input rotation by a factor of 10^{-1} .The seismic noise was calculated by multiplying its transfer function with a seismic activity dataset, which resulted in the lowest seismic noise as $10^{-14}\ rad/\sqrt{Hz}$ for quiet conditions and the highest of $10^{-13}\ rad/\sqrt{Hz}$ for windy conditions. The thermal noise was calculated to be $10^{-19}\ rad/\sqrt{Hz}$. The lower the centre of mass offset value, the value of seismic noise decreases. Furthermore, a high quality factor and a reduced flexure stiffness decreased the thermal noise.

1 Introduction

Horizontal seismometers and tiltmeters can measure the platform acceleration and are also sensitive to tilt due to the effect of gravity on the device[13]. However, they cannot distinguish successfully due to their design which behaves like a spring-mass system or a vertical pendulum[1]. This coupling is especially evident at low frequencies, which behaves as a limitation of the system, so inertial sensors prove to be efficient in isolating the platforms from ground motion [13]. The beam rotation sensor is a device that can decouple platform acceleration and ground rotation due to its design, which consists of a beam suspended on a pair of flexures, staying inertial at frequencies above the resonant frequency of the system[1]. Furthermore, signal to noise ratio determines the efficacy of the system and should be higher to obtain optimal event rates in gravitational detectors [9].

The thermal noise dominates in frequencies less than 100 Hz [14], which arises due to the mechanical dissipation in materials such as flexures[10]. The thermal noise is measured using the fluctuation-dissipation theorem using instrument parameters such as mechanical loss, resonant frequency and temperature[14]. The behaviour of the beam rotation sensor in low frequencies is measured by computing the transfer function as a ratio of input rotation and the output value measured by the auto-collimator. The seismic noise is also calculated by computing the transfer function but as a ratio of platform rotation and acceleration to get the magnitude of the coupling[1].

Since this transfer function only provides the coupling, when multiplied by the power spectral density of seismic data, it gives the value of seismic noise. The improvement in signal to noise ratio can be achieved by changing parameters of the rotation sensors such as the stiffness of the flexure, centre of mass offset, and quality factor to observe the effect on seismic and thermal noise in the beam rotation sensor.

2 Background Theory

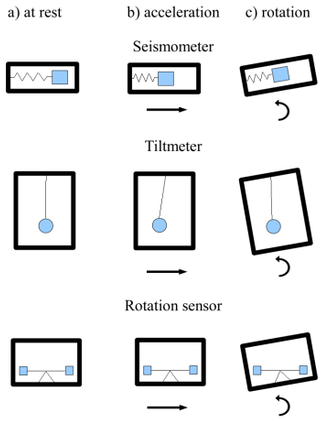

Figure 1: The working principle of seismometer and tiltmeter in comparison to the beam rotation sensor[1].

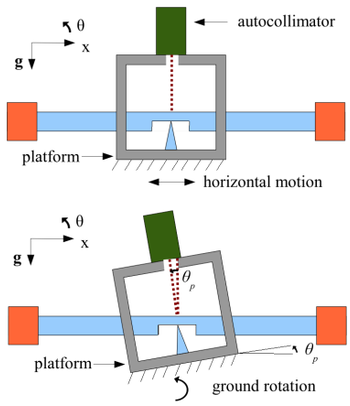

Figure 2: The beam balance measures the rotation using the autocollimator with respect to its platform[1].

Tiltmeters work in the principle that vertical pendulums and horizontal seismometers behave like a spring-mass system, making both the devices sensitive to horizontal acceleration and ground rotation[7][1]. They can give the rotation of a line segment fixed in a specific axis about a horizontal axis perpendicular to the weight of the system [7]. However, they are unable to successfully distinguish the platform acceleration and ground rotation because, in an inertial frame, the acceleration and the rotation produce the same output [1]. The beam rotation sensor consists of a beam suspended on a pair of notch type flexures as shown in figure 2, enabling the system to distinguish the two motions optimally due to the beam balance, compared to the horizontal seismometer or a tiltmeter, as shown in figure 1 [1]. The ground rotation is measured by calculating the angle between the beam balance and the autocollimator with respect to the platform [1], where the centre of mass is close to the pivot, as shown in figure 2.

Flexures are bearings used with loads such as beams to allow the bending in a preferred way with degrees of freedom and degrees of constraint, having functional requirements such as stiffness and load capacity[11]. Notch type flexures are compliant flexure pivot that allows for a single axis rotation[12]. Seismic noise arises when measuring low frequency below 100 Hz in the gravitational detectors due to seismic activity [9]. The detector usually measures the displacement at a significantly higher magnitude than the order of seismic noise, which is calculated to be 10^{-16} rms. Therefore, a reduction in seismic noise is required to produce an accurate event rate[9]. The thermal noise is caused by the Brownian noise, which occurs due to the high mechanical dissipation in materials used in the detectors[10].

3 Beam rotation sensor (BRS)

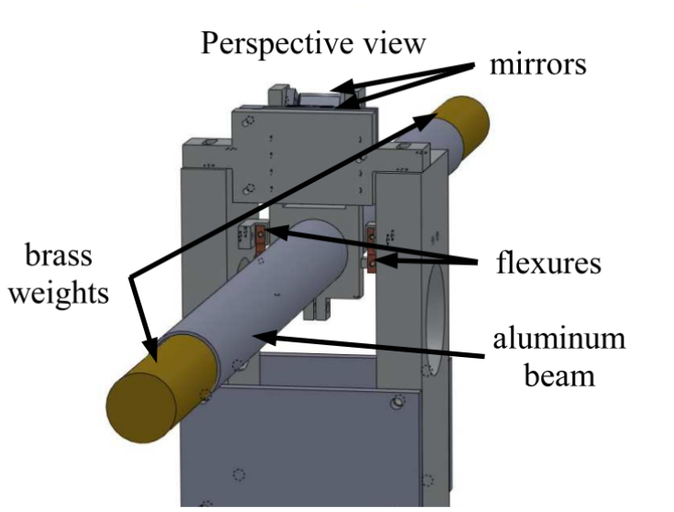

Figure 3: The schematic model of the beam rotation sensor and its components[1].

3.1 Flexures

The beam rotation sensor is suspended by a pair of flexures,as shown in figure 3, staying in an inertial frame at frequencies above the resonance frequency of the balance. The flexures are notch type flexures made of beryllium-copper alloy, as shown in figure 4, with a thickness of 25±2 m, a radius of 3.2 mm, and a width of 6.3 mm , as represented by figure 5 [1]. These flexures are aged in atmospheric air at 300°C for two hours to harden the flexures and obtain an optimum stress level yield, thus improving its ability to withstand high static loads and boosting the system's performance [2].

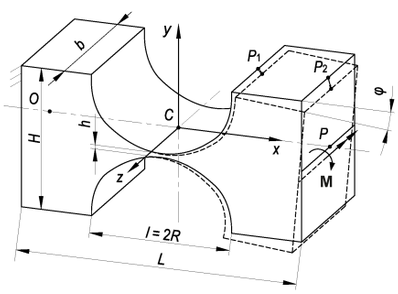

Figure 4: Model of a notch type flexure hinge with its geometric parameters[3].

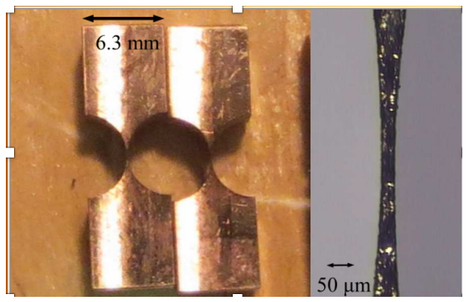

Figure 5: A pair of beryllium-copper alloy flexures used in the BRS[1].

3.2 Equation of motion

The BRS was modelled as a simple pendulum to calculate its equation of motion, which aids in determining its transfer function and the noise of the system. This equation was computed by examining the external and internal torque. The internal torque includes the torque due to the stiffness of the flexure, the torque due to the weight applied with a horizontal offset between the centre of mass and the pivot, and the torque due to the acceleration force; applied with a vertical offset between the centre of mass and the pivot.

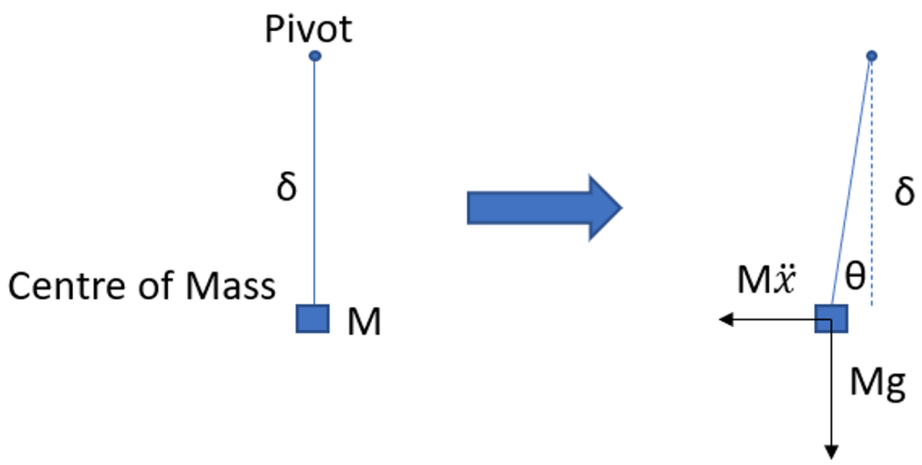

Figure 6: BRS modelled as a simple pendulum to obtain the equation of motion.

$$I\ddot{\theta} + \kappa_e(1 + i\phi)(\theta - \theta_p) + Mg\theta\delta + M\ddot{x_p}\delta = \tau \tag{1}$$

where I is the Moment of inertia , κ_e is the flexure angular stiffness , θ is the angle between the beam and the inertial frame's horizontal plane , θ_p is the platform rotation angle , M is the mass of the system , δ is the centre of mass offset and, τ is the external torque.

3.3 Transfer function

The transfer function provides the relationship between the output value of a dynamical system with the given input value as a function of frequency[4]. The transfer function was calculated as the ratio of the input motion of the ground to the output value of the system as represented by Equation 2; this allows us to understand how the BRS measures ground rotation and platform acceleration. Firstly, the external torque and acceleration were set to zero, and the equations of motion were rearranged into a standard oscillator equation, represented by Equation 1. Secondly, the resonant frequency was calculated to be 0.01 Hz by substituting the parameters of the BRS. Since the system stays inertial above the resonant frequency of the balance, the frequency range for observing the system's behaviour was set from 10^{-3} Hz to 10^{-1} Hz.

$$\frac{|\theta - \theta_p|}{|\theta_p|} = \frac{|\omega^2 - \omega_g^2|}{\sqrt{(\omega^2 - \omega_0^2)^2 + \frac{\omega_0^4}{Q'^2}}} \tag{2}$$

Where $\omega_0^2 = \frac{\kappa_e + Mg\delta}{I}$, $\omega_g^2 = \frac{Mg\delta}{I}$, $Q' = \frac{\kappa_e + Mg\delta}{\kappa_e}$.

where I is the Moment of inertia , κ_e is the flexure angular stiffness , θ is the angle between the beam and the inertial frame's horizontal plane , θ_p is the platform rotation angle , M is the mass of the system , δ is the centre of mass offset and, τ is the external torque.

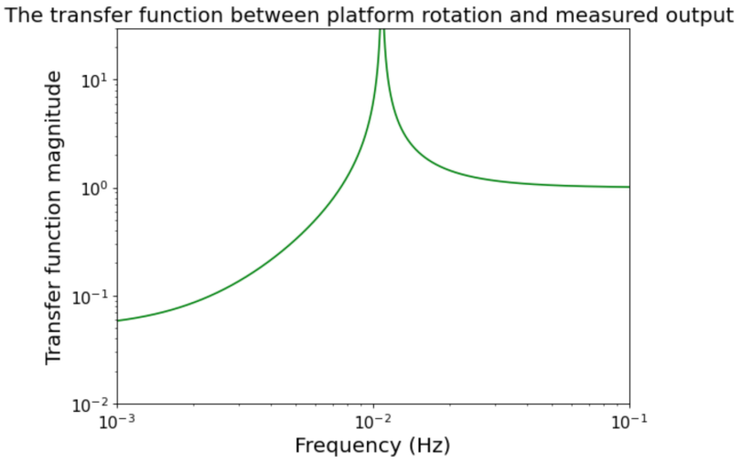

Figure 7: The plot of the output value of the system for the input ground rotation as a function of frequency.

The magnitude of the transfer function was plotted on python for the frequency range as shown in Figure 7. The transfer function gave an output of 1 above the resonant frequency, implying the system outputs the exact value of ground rotation for the given input value. However, below the resonant frequency, a continuous decline in the transfer function value was observed, which suggests that the rotation value measured by the system is less than the input.

4 Seismic Noise

4.1 Transfer function

The transfer function, which provides the coupling between the ground rotation and the platform acceleration, was required to calculate the seismic noise to analyse how the system could distinguish the two motions. Equation 3 gives the magnitude of the ratio of the platform acceleration to the ground rotation function.

$$\frac{\theta}{\dot{x}} = \frac{M\omega^2\delta}{I(\omega^2 - \omega_0^2 - i\frac{\omega_0^2}{Q'})} \tag{3}$$

where I is the Moment of inertia , κ_e is the flexure angular stiffness , θ is the angle between the beam and the inertial frame's horizontal plane , θ_p is the platform rotation angle , M is the mass of the system , δ is the centre of mass offset and, τ is the external torque.

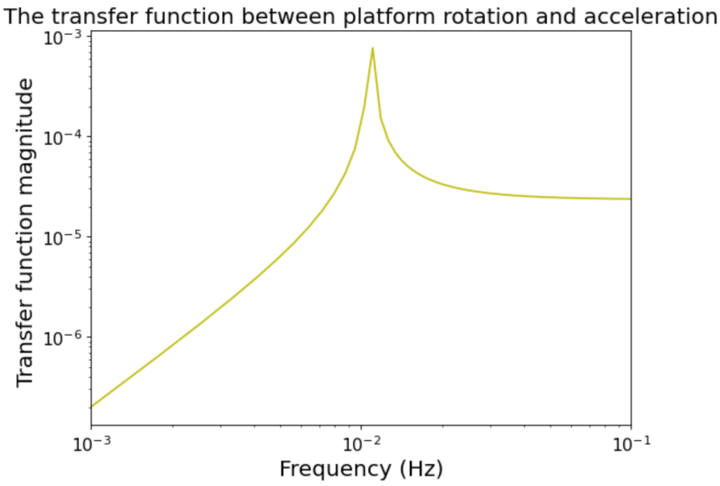

Figure 8: The coupling between the ground rotation and platform acceleration as a function of frequency.

The coupling was plotted as a function of the frequency range given by figure 8. The transfer function was calculated to be $6 * 10^{-5}$ for the given parameters of BRS above the resonant frequency of the system. However, below the resonant frequency, the system is inconsistent as expected. Therefore, the value of ground rotation measured when coupled with the platform acceleration provides a much higher rotation value at low frequencies.

4.2 Analysing data to find the seismic noise

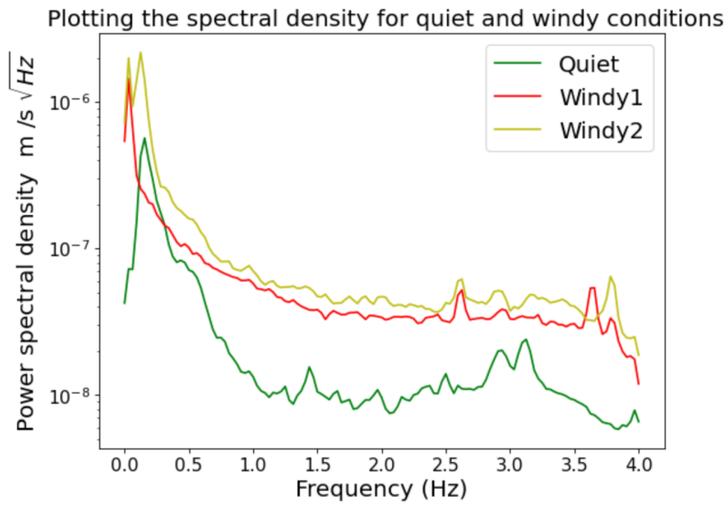

Figure 9: The power spectral density plotted as a function of frequency for seismic activity dataset .

The seismic noise was calculated by multiplying the transfer function (Equation 3) by the power spectral density of a dataset. This dataset contained the wind's velocity as a function of time; this then had to be converted to a frequency domain using the pwelch function on python to obtain the power spectral density, as shown in figure 9. Furthermore, the seismic noise was plotted in figure 10 for the frequency range of 10^{-3} Hz to 10^{-1} Hz, to gain insight into the impact of wind speed on seismic noise. The value of seismic noise increased when the velocity of the wind was higher, and the lowest value was observed for quiet conditions, which was calculated to be 10^{-14} $rad/\sqrt{Hz}$.

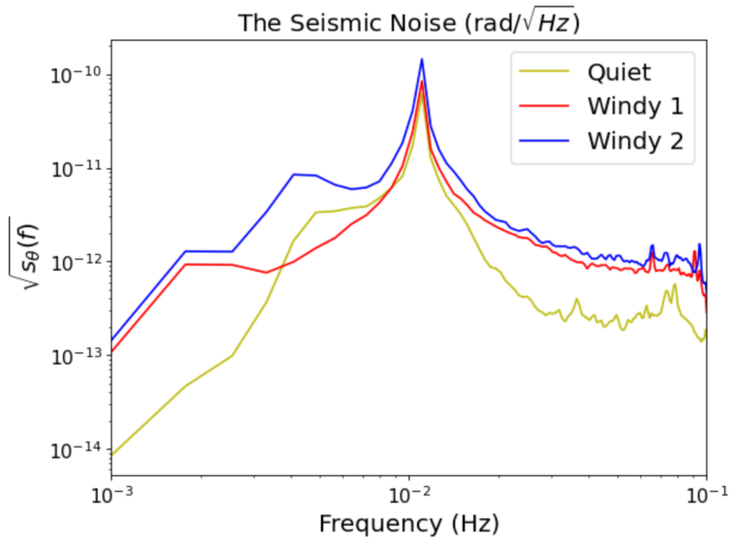

Figure 10: The seismic noise plotted as a function of frequency for quiet and windy conditions.

5 Thermal Noise

The thermal noise is an intrinsic property of the system that limits the sensor's sensitivity, estimated using the Fluctuation-Dissipation Theorem by relating its fluctuations in terms of mechanical displacement with impedance (FDT)[5][6]. The power spectral density of the displacement (Equation 4) as a function was frequency was calculated by taking the real part of the mechanical admittance through evaluating the motion of a damped harmonic oscillator[6].

$$S_\theta(\omega) = \frac{4k_b t\kappa\phi}{\omega[(I\omega^2 - \kappa - Mg\delta + \omega^2\delta M)^2 + \kappa^2\phi^2]} \tag{4}$$

where I is the Moment of inertia , κ_e is the flexure angular stiffness , θ is the angle between the beam and the inertial frame's horizontal plane , θ_p is the platform rotation angle , M is the mass of the system , δ is the centre of mass offset and, τ is the external torque.

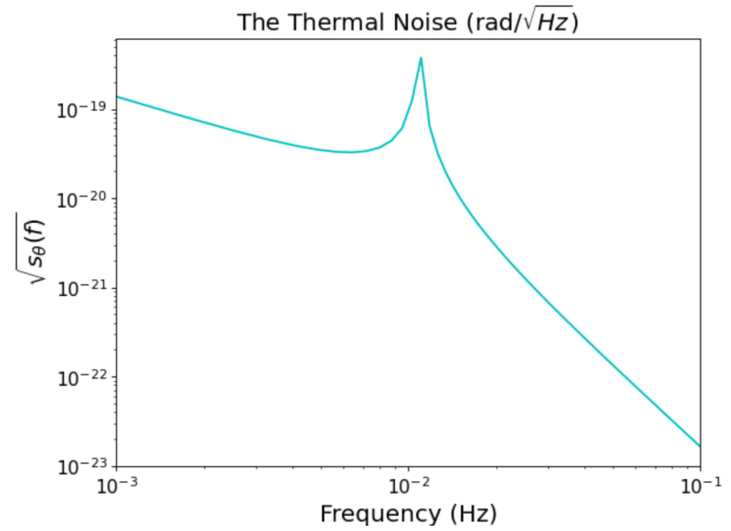

Figure 11: The power spectral density of mechanical displacement as a function of frequency.

The thermal noise was plotted as a function of frequency, as shown in figure 11. The value of thermal noise was calculated to be 10^{-19} $rad/\sqrt{Hz}$ below the system's resonant frequency, which is significantly less than seismic noise. As observed in seismic noise, the thermal noise increases with lower frequencies.

6 Improving signal to noise ratio

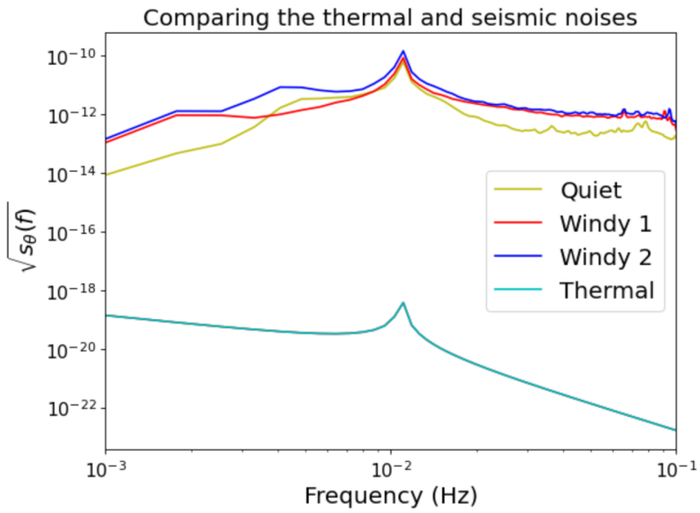

Figure 12: Plotting the seismic and thermal noise.

The seismic and thermal noise are represented in Figure 12 to analyse the signal to noise ratios, which can be improved by reducing the noise. This reduction in the seismic noise provides a significant advantage when measuring the ground rotation, or platform acceleration, as the seismic noise is the first limitation that is immediately observed at low frequencies.

Parameters of the BRS such as the centre of mass offset, quality factor, and stiffness of the flexure all play vital roles in reducing the noise in the system, as demonstrated by Equations 3 and 4. Therefore, a range of values for these parameters was input in the equations to observe the behaviour of the system in terms of its signal to noise ratio (SNR). Although some quantities such as the mass of the balance (m) and moment of inertia (I) did not provide a significant improvement in thermal noise, it affected the seismic noise, and the centre of mass offset was susceptible to the seismic noise at low frequencies[1]. Firstly, a perfectly balanced system achieved a higher SNR in terms of seismic noise by decreasing the centre of mass offset by reducing the value closer to zero, as shown in Figure 13. Secondly, the lower the damping of the oscillator gives a higher quality factor [7] which corresponds to reduced thermal noise at low frequencies, as shown in Figure 14. Finally, the stiffness of the flexure affected only the thermal noise, as expected from Equation 4.

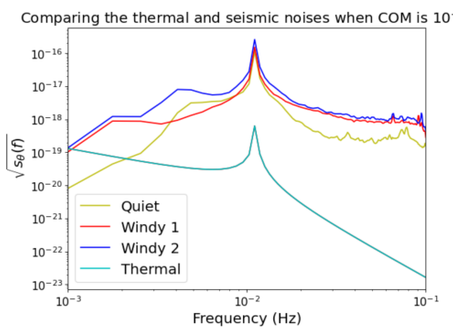

Figure 13: Seismic noise reduction due reducing the centre of mass offset.

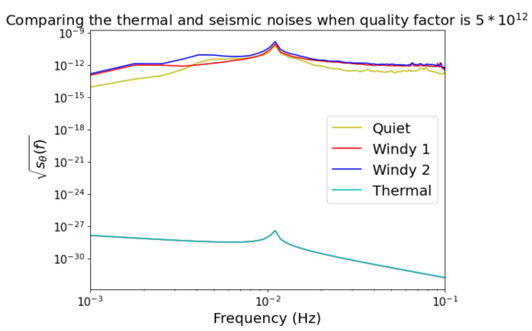

Figure 14: Thermal noise reduction due to increasing the quality factor.

Firstly, a balanced system achieved a higher SNR in seismic noise, calculated to be 10^{-20} $rad/\sqrt{Hz}$. This was acquired by decreasing the centre of mass offset by reducing the value to 10^{-12} μm, as shown in Figure 13. Secondly, the lower the damping of the oscillator gives a higher quality factor [7] which corresponds to reduced thermal noise at low frequencies. Therefore, the thermal noise improved to 10^{-27} $rad/\sqrt{Hz}$ when the quality factor was increased to $5 * 10^{12}$, as shown in Figure 14. Finally, the stiffness of the flexure affected only the thermal noise, as expected from Equation 4.

7 Conclusion

The beam rotation sensor is able to distinguish the coupling between platform acceleration and ground rotation compared to a horizontal seismometer or a tiltmeter. The equation of motion of this instrument provided the internal and external torque acting on it, which included the parameters of the balance such as the Moment of inertia (I), flexure angular stiffness (k), and the centre of mass offset (δ). The transfer function was computed as a ratio of the input rotation to the output measured by the autocollimator. The resulting value was one above the resonant frequency and 10^{-1} Hz below the resonant frequency suggesting that the system measures a lower rotation value for frequencies below the resonant frequency of the system. Furthermore, the transfer function for the coupling between the tilt-acceleration was computed to obtain the seismic noise. The resulting value of $6 * 10^{-5}$ above resonant frequency and a steady decline in transfer function below resonant frequency was measured. Therefore, the coupling increases at lower frequencies which manifests as seismic noise.

The seismic noise was obtained from the transfer function by multiplying the power spectral density of a seismic activity dataset containing the velocity of the wind as a function of time. It was observed that the seismic noise was the lowest for quiet conditions, and the noise increases as a function of wind speed which corresponds to a comparatively higher seismic activity. The lowest seismic noise was calculated to be 10^{-14} $rad/\sqrt{Hz}$, and the highest was 10^{-13} $rad/\sqrt{Hz}$.Moreover, the thermal noise caused by Brownian motion was calculated using the fluctuation-dissipation theorem by taking the admittance of the system, which is calculated to be 10^{-19} $rad/\sqrt{Hz}$.The thermal noise was relatively lower than the seismic noise, implying that the dominant noise that affects the event rate at low frequencies is seismic noise.

The signal-to-noise ratio was increased by changing various parameters of the balance, such as the centre of mass, stiffness of the flexure, and the quality factor. The centre of mass affected the seismic noise by reducing the noise to 10^{-20} $rad/\sqrt{Hz}$ when it was decreased from 10^{-3} μm to 10^{-12} μm. The thermal noise was affected by the stiffness of the flexure due to mechanical dissipation. The quality factor improved the thermal noise to 10^{-27} $rad/\sqrt{Hz}$ when it was increased to $5 * 10^{12}$.

8 References

1. Venkateswara, K., Hagedorn, C. A., Turner, M. D., Arp, T., Gundlach, J. H. (2014). A high-precision mechanical absolute-rotation sensor. Review of Scientific Instruments, 85(1), 015005. https://doi.org/10.1063/1.4862816

2. Clark, D., Lantz, B. (2009). Replacement Flexures for the GS-13 Seismometer For use by the LIGO Seismic Isolation sub-system on the BSC and HAM in vacuum seismic isolation platforms (LIGO-T0900089 ed., Vol. 1). Stanford University. https://dcc.ligo.org/public/0000/T0900089/001/T0900089-v1.pdf

3. Torres Melgarejo, M., Darnieder, M., Linß, S., Zentner, L., Fröhlich, T., Theska, R. (2018). On Modeling the Bending Stiffness of Thin Semi-Circular Flexure Hinges for Precision Applications. Actuators, 7(4), 86. https://doi.org/10.3390/act7040086

4. x-engineer.org. (n.d.). How to find the transfer function of a system – x-engineer.org. How to Find the Transfer Function of a System. Retrieved January 10, 2022, from https://x-engineer.org/transfer-function/

5. Fontana, A., Pedurand, R., Dolique, V., Hansali, G., Bellon, L. (2021). Thermal noise of a cryocooled silicon cantilever locally heated up to its melting point. Physical Review E, 103(6). https://doi.org/10.1103/physreve.103.062125

6. Masso Herrera, M. (2019). Properties of bonded silicon for future generations of gravitational wave observatories. https://theses.gla.ac.uk/41177/1/M.MassoHerrera$_PhD.pdf$

7. Fitzpatrick, R. (2008, April 8). Quality Factor. University of Texas. Retrieved December 22, 2021, from https://farside.ph.utexas.edu/teaching/315/Waves/node11.html

8. Goulty, N. R. (1976). Strainmeters and tiltmeters in geophysics. Tectonophysics, 34(3–4), 245–256. https://doi.org/10.1016/0040-1951(76)90099-8

9. Stochino, A., DeSalvo, R., Huang, Y., Sannibale, V. (2007). Improvement of the seismic noise attenuation performance of the Monolithic Geometric Anti-Spring filters for gravitational wave interferometric detectors. Nuclear Instruments and Methods in Physics Research Section A: Accelerators, Spectrometers, Detectors and Associated Equipment, 580(3), 1559–1564. https://doi.org/10.1016/j.nima.2007.06.029

10. Tugolukov, M., Levin, Y., Vyatchanin, S. (2018). Thermal noise computation in gravitational wave interferometers from first principles. Physics Letters A, 382(33), 2181–2185.

https://doi.org/10.1016/j.physleta.2017.07.001

11. Thomas, M. (n.d.). Flexures. MIT. Retrieved January 2, 2022, from https://web.mit.edu/mact/www/Blog/Flexures/FlexureIndex.html

12. Koppen, S., Langelaar, M., van Keulen, F. (2021, October 8). A simple and versatile topology optimization formulation for flexure synthesis. Cornell University. Retrieved January 5, 2022, from https://arxiv.org/pdf/2111.04620.pdf

13. Matichard, F., Evans, M. (2015). Review: Tilt-Free Low-Noise Seismometry. Bulletin of the Seismological Society of America, 105(2A), 497–510. https://doi.org/10.1785/0120140200

14. Hammond, G. D., Cumming, A. V., Hough, J., Kumar, R., Tokmakov, K., Reid, S., Rowan, S. (2012). Reducing the suspension thermal noise of advanced gravitational wave detectors. Classical and Quantum Gravity, 29(12), 124009. https://doi.org/10.1088/0264-9381/29/12/124009